Received 8 October 2021; revised 8 November 2021; accepted 18 November 2021. Date of publication 23 November 2021;
date of current version 2 December 2021.

Digital Object Identifier 10.1109/OJAP.2021.3130208

A Low-Profile Dual-Band Filtering Hybrid Antenna With Broadside Radiation Based on Patch and SIW Resonators

QIANWEN LIU [1,2] AND LEI ZHU [3] (Fellow, IEEE)

[1]College of Telecommunications and Information Engineering, Nanjing University of Posts and Telecommunications, Nanjing 210003, China
[2]National and Local Joint Engineering Laboratory of RF Integration and Micro-Assembly Technology,
Nanjing University of Posts and Telecommunications, Nanjing 210003, China
[3]Department of Electrical and Computer Engineering, Faculty of Science and Technology, University of Macau, Macau, China
CORRESPONDING AUTHOR: Q. LIU (e-mail: aliuqw@163.com)

This work was supported in part by the National Nature Science Foundation of China under Grant 61971475 and Grant 62101279; in part by Nanjing University of Posts and Telecommunications Scientific Foundation (NUPTSF) under Grant NY221010 and Grant NY217002; and in part by the Open Research Fund of the National and Local Joint Engineering Laboratory of RF Integration and Micro-Assembly Technology under Grant KFJJ20200205.

ABSTRACT This paper presents a differentially fed dual-band hybrid antenna with broadside radiation, enhanced bandwidth, and high selectivity. The proposed antenna is constructed using a single- layer substrate based on rectangular patch resonator and substrate integrated waveguide (SIW) cavity. Herein, TM_{10} and TM_{12} modes of the rectangular patch resonator, together with TE_{21} and TE_{23} modes of the rectangular SIW cavity, are selected for resonances in the concerned dual-band radiation. Among them, TM_{10} and TE_{21} are employed for the lower passband, while TM_{12} and TE_{23} for the higher passband. Besides, for achieving broadside radiation performances in both bands, two arrays of shorting pins are loaded in the rectangular patch resonator and the constituted electric wall surround the rectangular SIW cavity is properly truncated to reshape the radiation patterns of TM_{12} and TE_{23}, respectively. Notably, the resonant and radiation properties of all the involved modes are obtained with theoretical deduction. Furthermore, the cascaded trisection composed of the SIW cavity, the patch resonator, and the radiation impedance creates two radiation nulls in each upper stopband of both passbands and the mixed coupling between two resonators generates another radiation null to be located in the lower stopband of the higher passband. For demonstration, a prototype antenna with the dual bands at 3.5 and 5.8 GHz is fabricated and tested. The measured results show that the antenna has achieved an improved bandwidth ($|S_{dd11}| < -10$ dB) from 3.26 to 3.58 GHz and 5.60 to 5.90 GHz, respectively, with stable broadside gains of around 8.5 dBi. In addition, in the stopband, three radiation nulls are created at 3.71, 5.32, and 6.12 GHz for effective enhancement of dual-band frequency selectivity.

INDEX TERMS Bandwidth enhancement, dual-band antenna, high selectivity, radiation pattern reshaping, single-layer.

I. INTRODUCTION

IN WIRELESS communications, various antennas have been recently developed towards versatility in performances and miniaturization in size. Given this, the dual-band antennas can effectively reduce their element number and overall volume as highly demanded and extensively studied nowadays.

For realizing dual-band performance, various techniques based on multiple modes or resonators are often employed, and they can be in general classified into two main categories. The first kind is introducing extra resonators to obtain extra resonances. In this context, multiple resonators with varied configurations, such as parasitic patch resonators [1]–[6], slot resonators [7], [8], and stubs [9], [10], are adopted, and they are placed in proximity to the core radiator. As multiple resonators are used, the complexity of resultant antennas inevitably gets increased. To overcome this drawback, the second one is

This work is licensed under a Creative Commons Attribution 4.0 License. For more information, see https://creativecommons.org/licenses/by/4.0/

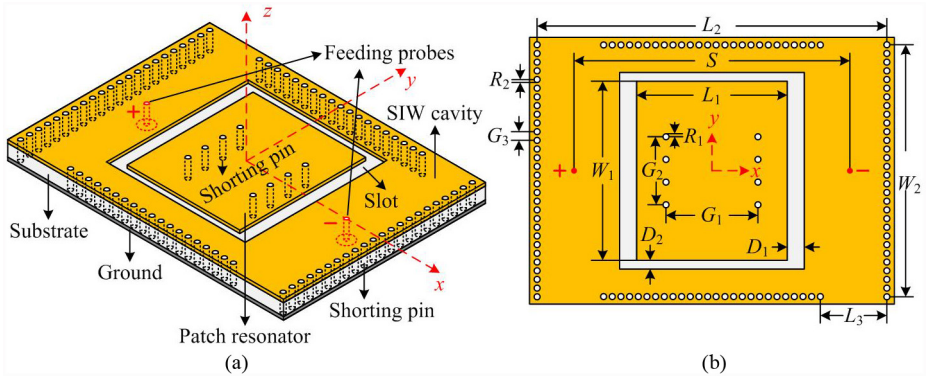

FIGURE 1. Geometry of the proposed dual-band filtering antenna. (a) 3-D view. (b) Side view.

proposed by exciting multiple resonant modes in a single resonator [11]–[20]. However, due to the diversity among different modes, diverse radiations are often produced in these two bands even though the dual-band dual-linear-polarized antenna with stable gain is highly required in many cases.

Apart from the in-band properties, many research works are carried out on improvement of the out-of-band performances by integrating the filtering function into the dual-band antenna design for reduction of their overall size and loss. In general, the filtering antenna is basically realized by co-designing the filter and antenna into a single block [21]–[23]. This design principle needs to employ extra filter structures, so as to enlarge the antenna size or bring in extra insertion loss. For this reason, an alternative method has been proposed to realize the filter function by modifying the antenna feeding network. In this case, a variety of designs with multi-stub microstrip feed line [24], extended feeding probe [25], T-shaped coupled microstrip line [26], and copper top hat [27] are developed and reported. In these designs, the radiation nulls are obtained by blocking the signal from transmission in the feeding structure at specific frequencies. However, there still exist a few disadvantages, such as the increased complexity and extra loss from the feeding network. Therefore, some filtering antennas without any extra circuit are proposed by fusing the filter function into the radiator itself. For instances, a few improved works are well done by introducing slots [25], [28], parasitic patches [28], and via holes [29], [34]. Besides, reshaping or adjusting the radiation pattern [27] is also considered as an effective way to obtain the radiation nulls. Herein, as the antenna radiator is equipped with the filtering capability, the overall size can be effectively reduced and the radiation performance can be enhanced as well. Nevertheless, it is still a challenging task to attain the desired in-band radiation performances and good out-of-band rejection simultaneously.

In this paper, a compact dual-band filtering antenna constructed using a single layer structure is proposed. In this design, the rectangular patch resonator and substrate integrated waveguide (SIW) cavity are both adopted. Initially, based on the analysis of the adopted two resonators, TM_{10} and TM_{12} modes of the rectangular patch resonator, together with TE_{21} and TE_{23} modes of the rectangular SIW cavity are selected to realize the dual resonances in each band. Afterwards, the two resonators are combined and modified to transform the non-broadside radiation of TM_{10} and TM_{12} into the broadside radiation, ensuring consistent radiation on both bands. Meanwhile, the specific coupling property between adopted resonators and the radiation mechanism create three radiation nulls near the passbands. The remainder of this paper is organized as follows. Section II illustrates the working mechanisms about how to form two passbands with same radiation performance and produce three radiation nulls by combination of two resonators. In Section III, a prototype antenna is fabricated and its measured results are performed. Finally, a conclusion is presented.

II. GEOMETRY AND WORKING MECHANISM

The antenna is designed and fabricated on a single-layer Rogers 5880 substrate with a permittivity of $\varepsilon_r = 2.33$ and a thickness of $H = 3.175$ mm. Fig. 1 depicts the geometry of the proposed dual-band antenna, which consists of a rectangular patch resonator, a rectangular SIW cavity, and a pair of differential feeding ports. Different from the conventional resonators, two arrays of shorting pins are loaded in the adopted rectangular patch resonator. Meanwhile, a rectangular aperture is etched in the middle of the rectangular SIW cavity to contain the rectangular patch resonator and a certain part of surrounded metallic pins are removed. Moreover, a pair of differential feeding probes is distributed in the rectangular SIW cavity. Table 1 tabulates the dimensions of the proposed antenna. To improve the efficiency and accuracy, the scientific calculator MATLAB combined with the electromagnetics (EM) simulator high frequency structure simulator (HFSS) are used in the design procedure. In the following, the antenna in Fig. 1 is extensively studied and the same geometrical parameters in Table 1 are used during analysis unless otherwise stated. Firstly, the patch resonator and SIW cavity are separately investigated. After that, these two types of resonators are reshaped and combined with each other for achievement of desired performances. Last but

TABLE 1. Dimensions of the proposed antenna in Fig. 1.

Parameter	Value (mm)
L_1	36.5
W_1	42.6
L_2	81.6
W_2	58.4
S	65.4
D_1	5.6
D_2	1
G_1	21.6
G_2	17.4
R_1	0.3
L_3	15.5
R_2	0.3
G_3	0.9

not least, the coupling matrices of the proposed antenna are extracted for further clarification of the working mechanism.

A. MODE ANALYSIS OF PATCH RESONATOR AND SIW CAVITY

As the rectangular patch resonator and SIW cavity are essential components of the designed antenna, the electric field distributions of the two resonators should be firstly investigated.

According to the cavity model theory, the electric field of TM_{mn} modes in the rectangular patch resonator can be expressed as [35]

$$E_z = A_{mn} \cos \frac{m\pi x}{L} \cos \frac{n\pi y}{W} \tag{1}$$

Besides, the electric field of TE_{mn} modes in the rectangular SIW cavity can be written as [36]

$$E_z = A_{mn} \sin \frac{m\pi x}{L} \sin \frac{n\pi y}{W} \tag{2}$$

where m and n are two nonnegative integers, and L and W stand for the length and width of the rectangular patch resonator or SIW cavity.

According to (1) and (2), the field distribution of resonant modes in the rectangular patch resonator and SIW cavity can be obtained. Herein, considering the antenna is differentially fed, only odd modes are generated. Hence, Fig. 2 gives the computed electric field distributions of the first two odd modes in the rectangular patch resonator and SIW cavity. It is seen that the central field of TE_{21}, as circled with the yellow dot line in Fig. 2(c), is similar to that of TM_{10}. Moreover, the electric field in the middle of TE_{23} mode is the same as that of TM_{12}. Due to the similarities in electric field distribution, it is feasible to excite TM_{10} and TE_{21} or TM_{12} and TE_{23} at the same time, thereby creating a potential in achieving dual-band performance with these four modes.

B. EVOLUTION PROCESS OF PROPOSED ANTENNA

Next, based on the field distributions of relevant modes, the working mechanism of the proposed antenna is explained towards the evolution process shown in Fig. 3.

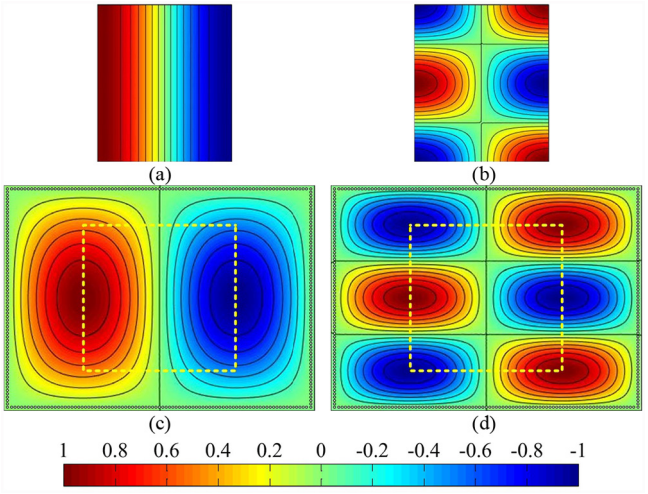

FIGURE 2. Computed electric field distributions. (a) TM_{10} and (b) TM_{12} in the rectangular patch resonator. (c) TE_{21} and (d) TE_{23} in the rectangular SIW cavity.

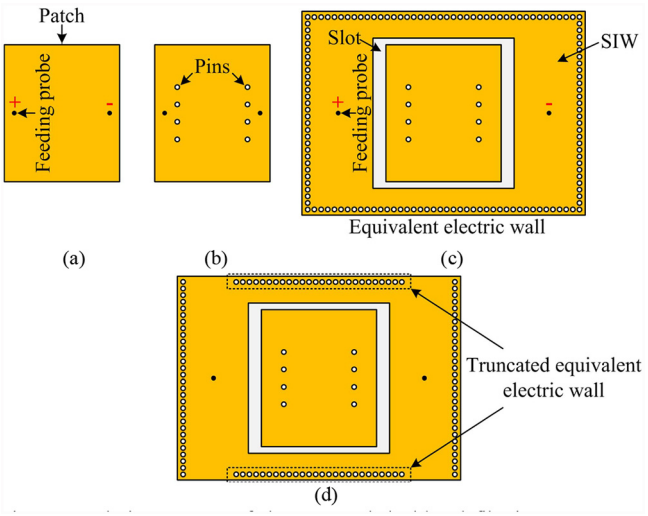

FIGURE 3. Evolution process of the proposed dual-band filtering antenna. (a) Antenna I: Rectangular patch antenna. (b) Antenna II: Pin-loaded rectangular patch antenna. (c) Antenna III: Combined antenna of pin-loaded rectangular patch resonator and SIW cavity. (d) Antenna IV: Combined antenna of pin- loaded rectangular patch resonator and electric-wall truncated SIW cavity.

1) ANALYSIS OF RECTANGULAR PATCH ANTENNA

The design starts with the conventional rectangular patch resonator shown in Fig. 3(a). It is known that the fundamental TM_{10} mode is equipped with the broadside radiation pattern while the higher TM_{12} mode produces the nonbroadside radiation pattern. Fig. 4 depicts the frequency responses of the conventional rectangular patch antenna, demonstrating that the radiation directivity at boresight direction is very low at the resonant frequency of TM_{10} and a radiation null exists around it. The null is produced by the radiation counteraction towards broadside direction of TM_{12} mode and it is confirmed by the radiation pattern of the frequency at the null shown in Fig. 4. For achieving a dual-band performance with stable radiation patterns with the combination of TM_{10}

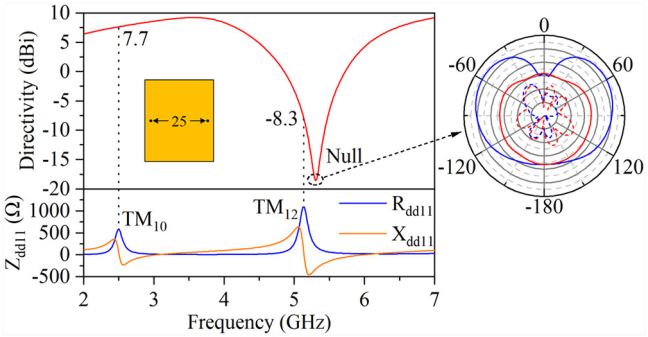

FIGURE 4. Simulated radiation directivity, input impedance, and radiation pattern of the conventional rectangular patch antenna.

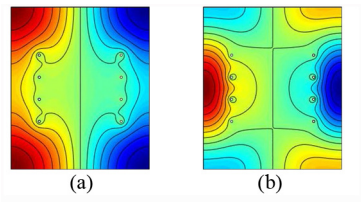

FIGURE 5. Computed electric field distributions of the pin loaded rectangular patch resonator. (a) Modified TM_{10}. (b) Modified TM_{12}.

mode, the non-broadside radiation of TM_{12} mode should be transformed into the broadside radiation.

Based on the fact that the radiation property is determined by the field distribution, radiation pattern can be properly reshaped. Fig. 2(b) illustrates the cancellation of radiation at boresight direction. As shown herein, the electric fields of TM_{12} vary twice along each radiating edge with equal magnitude. As such, two arrays of shorting pins are then loaded in the rectangular patch resonator to break down the symmetry as depicted in Fig. 3(b). For this modified patch resonator, the electric field should satisfy $E_{mn} = 0$ within the shorting pins, apart from the boundary condition $\partial E_{mn}/\partial n = 0$ of the conventional patch resonator. On the basis, by using the MATLAB PDE Toolbox, the field distribution and wave number of resonant modes in the pin-loaded rectangular patch resonator can be achieved. Fig. 5 depicts the computed electric field and it is seen that the field in the patch resonator gets changed. Herein, the resonant modes of the pin-loaded patch resonator are referred to as modified TM_{mn} corresponding to the TM_{mn} of the conventional patch resonator. As expected, the magnitude along radiation edges is no longer the same for both these two modes. Therefore, the radiation of modified TM_{12} will not be counteracted at boresight direction and thus a broadside radiation pattern is likely produced. Moreover, to confirm the broadside radiation of the modified modes, the radiation pattern is theoretically investigated.

The radiation pattern is expressed as

$$\begin{aligned} E_\theta &= jk_0\left(F_x \sin\varphi - F_y \cos\varphi\right) \\ E_\varphi &= jk_0\left(F_x \cos\varphi + F_y \sin\varphi\right)\cos\theta \end{aligned} \tag{3}$$

where F is the electric vector potential in the far zone and can be calculated from the electric field of the radiation boundaries as

$$F = \frac{h}{2\pi R} e^{-jk_0 R} \int_S \left(-\hat{n} \times \hat{z}E\right) e^{jk_0(x \sin\theta \cos\varphi + y \sin\theta \sin\varphi)} dxdy \tag{4}$$

Besides, the resonant frequency can be determined from the resonant wavenumber by

$$f_{mn} = \frac{c}{2\sqrt{\varepsilon_r}} k_{mn} \tag{5}$$

where k_{mn} is the wavenumber at resonance of TM_{mn}.

By using (3)-(5), the radiation patterns and resonant frequencies of the modified modes can be obtained. Figs. 6–9 plot the computed resonant properties of the modified patch resonator under different positions, dimensions, and numbers of the loaded shorting pins [30]. In general, the shorting pins have little influence on radiation of TM_{10}, and mainly affect TM_{12}. For TM_{12}, its boresight radiation is firstly enhanced and then reduced as the distance between two arrays (G_1) increases. This variation tendency is consistent with that of the length of array (G_2). Meanwhile, the number of shorting pins in each array (N) and the radius of pins (R_1) have relatively small impact on it. Moreover, the adopted shorting pins raise resonant frequencies of TM_{10} and TM_{12} ($f(TM_{10})$ and $f(TM_{12})$). Specifically, $f(TM_{10})$ goes up and $f(TM_{12})$ first rises then falls as G_1 increases from 0 to 30 mm. Also, $f(TM_{10})$ rises and $f(TM_{12})$ varies around 6.85 GHz when G_2 is enlarged to 30 mm. Both $f(TM_{10})$ and $f(TM_{12})$ rise slowly when R_1 increases. Besides, $f(TM_{10})$ keeps and $f(TM_{12})$ rises gradually when N increases.

Furthermore, the frequency responses of the pin-loaded rectangular MPA are also given and plotted in Fig. 10. It is revealed that the directivity at the frequency of TM_{12} has raised from −8.3 to 7.8 dBi. Meanwhile, there remains the null produced by virtue of field variation located at the lower frequency of modified TM_{12}.

2) COMBINATION OF PIN-LOADED PATCH AND SIW RESONATORS

After reshaping the resonant modes in the patch resonator, the antenna in Fig. 3(c) is constructed by embedding the pin loaded patch resonator in the rectangular SIW cavity for dual mode resonances in each band. As analyzed above, the first two odd modes of the SIW cavity, i.e., TE_{21} and TE_{23}, are utilized. Fig. 11 shows the simulated reflection coefficient, realized gain, and input impedance of the revised antenna. It is found that all desired modes are well generated and thus the expected bandwidth enhancement of both bands is achieved.

In addition, there are three radiation nulls near the two passbands. From the radiation patterns given in Fig. 11, it is observed that the nulls (Null 2 and 3) near the upper passband no longer exhibit non-broadside radiation. The disappearance of the null resulted by non-broadside radiation owing to the introduction of the SIW cavity. As the antenna composed of two radiators, at the frequency where the patch resonator

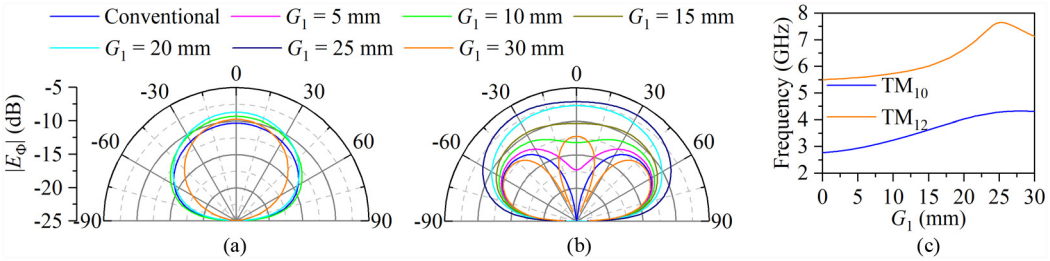

FIGURE 6. Theoretical analysis of the pin-loaded rectangular patch antenna with respect to the distance between two pin arrays (G_1). Radiation patterns of (a) modified TM_{10} and (b) TM_{12}. (c) Resonant frequencies of modified TM_{10} and TM_{12}.

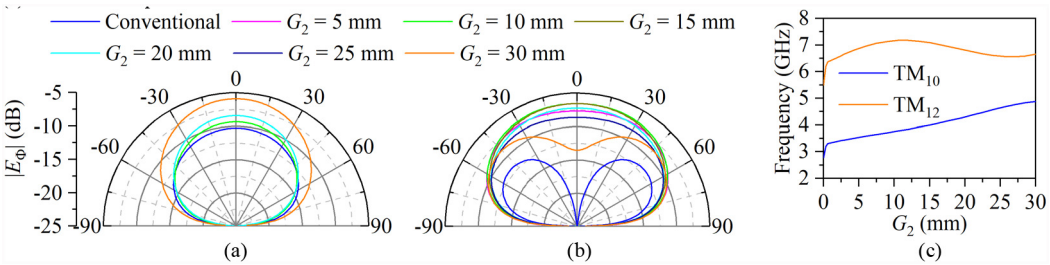

FIGURE 7. Theoretical analysis of the pin-loaded rectangular patch antenna with respect to the length of each pin array (G_2). Radiation patterns of (a) modified TM_{10} and (b) TM_{12}. (c) Resonant frequencies of modified TM_{10} and TM_{12}.

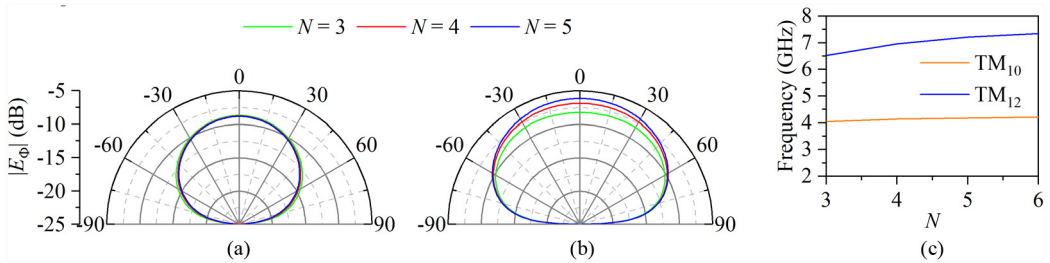

FIGURE 8. Theoretical analysis of the pin-loaded rectangular patch antenna with respect to the number of pins in each array (N). Radiation patterns of (a) modified TM_{10} and (b) TM_{12}. (c) Resonant frequencies of modified TM_{10} and TM_{12}.

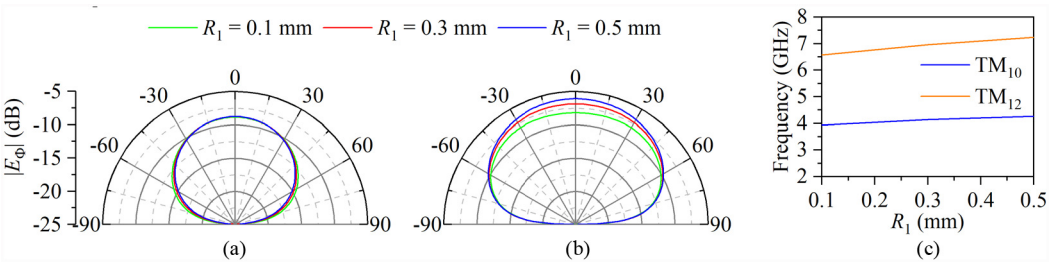

FIGURE 9. Theoretical analysis of the pin-loaded rectangular patch antenna with respect to the radius of pins (R_1). Radiation patterns of (a) modified TM_{10} and (b) TM_{12}. (c) Resonant frequencies of modified TM_{10} and TM_{12}.

exhibits non-broadside radiation, the other radiator, i.e., SIW cavity, will provide radiation in the broadside direction.

Besides, for the first null (Null 1) located in the upper stopband of the lower passband, although its radiation in broadside is lower, such slight decline is far from producing a deep null. The simulated field distributions in the antenna at radiation nulls shown in Fig. 12 are consistent with the above analysis. Herein, the nulls are produced by the coupling and radiation of the antenna. To clarify the principle, its equivalent coupling topology is derived and shown in Fig. 13. As depicted, the signal is input to the SIW cavity (R1) and then coupled to the inner patch resonator (R2). Specifically, a radiation impedance (L) is used to represent the radiation of the antenna. Referring to the synthesis theory for a filtering network, the cascaded trisection, which composed of three directly-coupled resonators with a cross coupling, results to produce an attenuation pole at finite frequency [37]. Herein, such a cascaded trisection is constructed with the R1, R2, and L, as shown in Fig. 13, and the resonant frequencies of the uncoupled resonators are denoted by f_{01} and f_{02} with

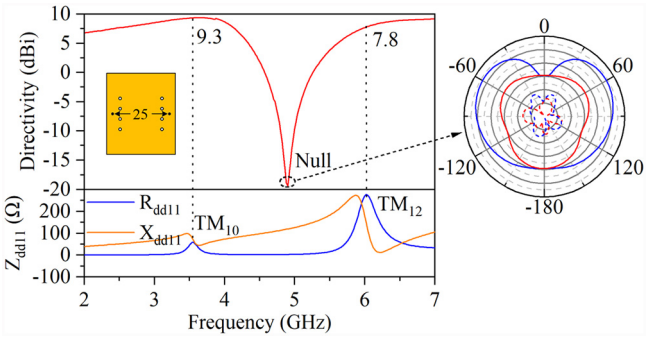

FIGURE 10. Simulated radiation directivity, input impedance, and radiation pattern of the pin loaded rectangular patch antenna.

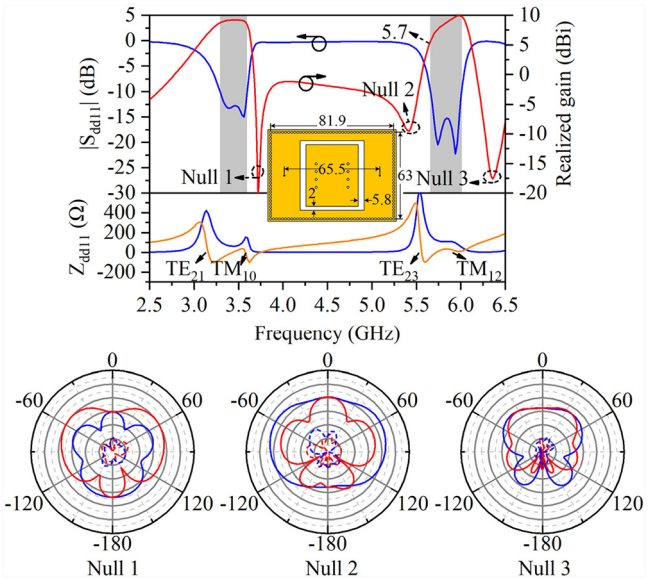

FIGURE 11. Simulated reflection coefficient, realized gain, input impedance, and radiation patterns of the combined antenna.

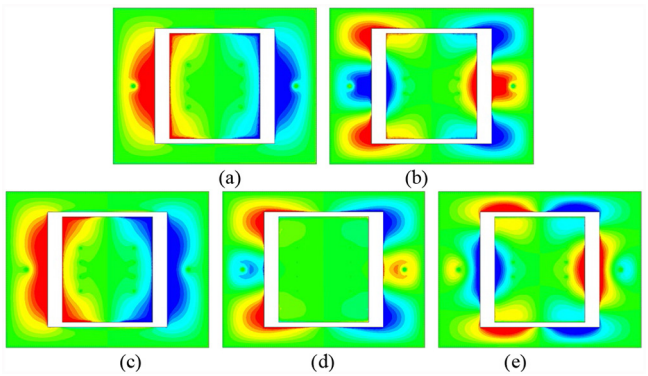

FIGURE 12. Simulated electric field distributions of the hybrid antenna. Center frequencies of (a) lower and (b) higher passbands. Frequencies of (c) Null 1, (d) Null 2, and (e) Null 3.

$f_{01} < f_{02}$. Accordingly, the two radiation nulls in the upper stopband of both bands (Null 1 and 3) can be explained. Besides, for the upper passband, as the electric field along the radiation boundaries of operation modes (modified TM_{12} and TE_{23}) have multiple periodic variations, both electric

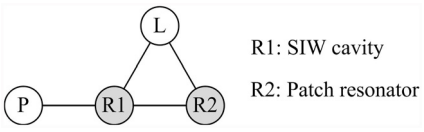

FIGURE 13. Coupling structure of the proposed antenna.

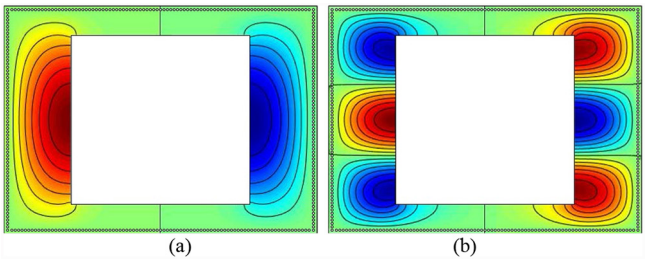

FIGURE 14. Computed electric field distributions of the rectangular SIW cavity with a rectangular aperture. (a) Modified TE_{21}. (b) Modified TE_{23}.

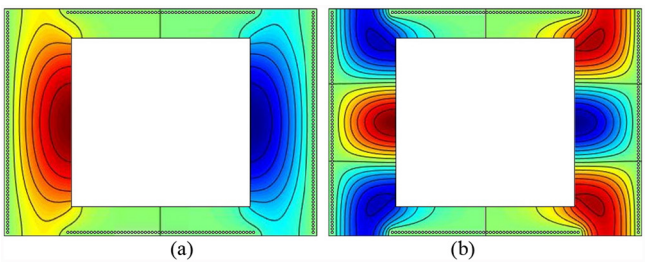

FIGURE 15. Computed electric field distributions of the rectangular SIW cavity with a rectangular aperture and truncated electric walls. (a) Modified TE_{21}. (b) Modified TE_{23}.

and magnetic couplings occur between these two resonators. Referring to the mixed coupling theory [31], [32], a transmission zero may be produced when electric and magnetic couplings exist simultaneously. Accordingly, the radiation null in the lower stopband of upper passband (Null 2) can be explained. Therefore, all radiation nulls are fully clarified now.

Except for the bandwidth and filtering performances, the radiation inside passbands should be concerned. Fig. 12 depicts the simulated electric field distributions at center frequencies of dual passbands, verifying the excitation of desired modes. However, the gain within the second passband at the resonant frequency of TE_{23} is slightly lower and is only 5.7 dB, so our further effort will be made in the following to improve it.

3) RADIATION PATTERN RESHAPING FOR TE_{23} MODE OF SIW CAVITY

As analyzed above, there exists certain similarity of field distribution between TM_{12} and TE_{23} modes. Hence, the low gain at the resonant frequency of TE_{23} is likely resulted by the same reason as confirmed by the computed electric field distributions of the rectangular SIW cavity shown in Fig. 14(b).

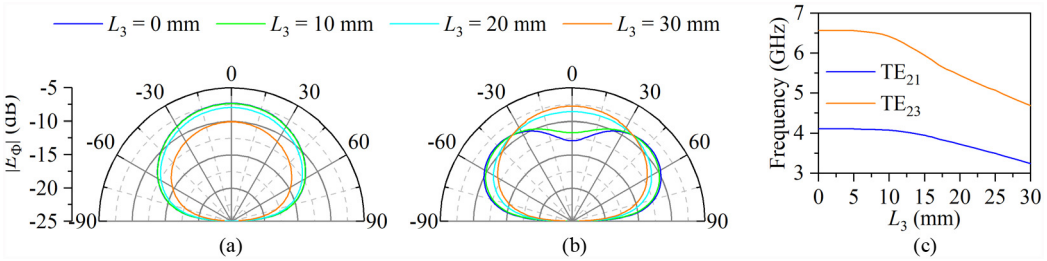

FIGURE 16. Theoretical analysis of the rectangular SIW cavity with a rectangular aperture and truncated electric walls with respect to the reduced electric wall length (L_3). Radiation patterns of (a) modified TE_{21} and (b) TE_{23}. (c) Resonant frequencies of modified TE_{21} and TE_{23}.

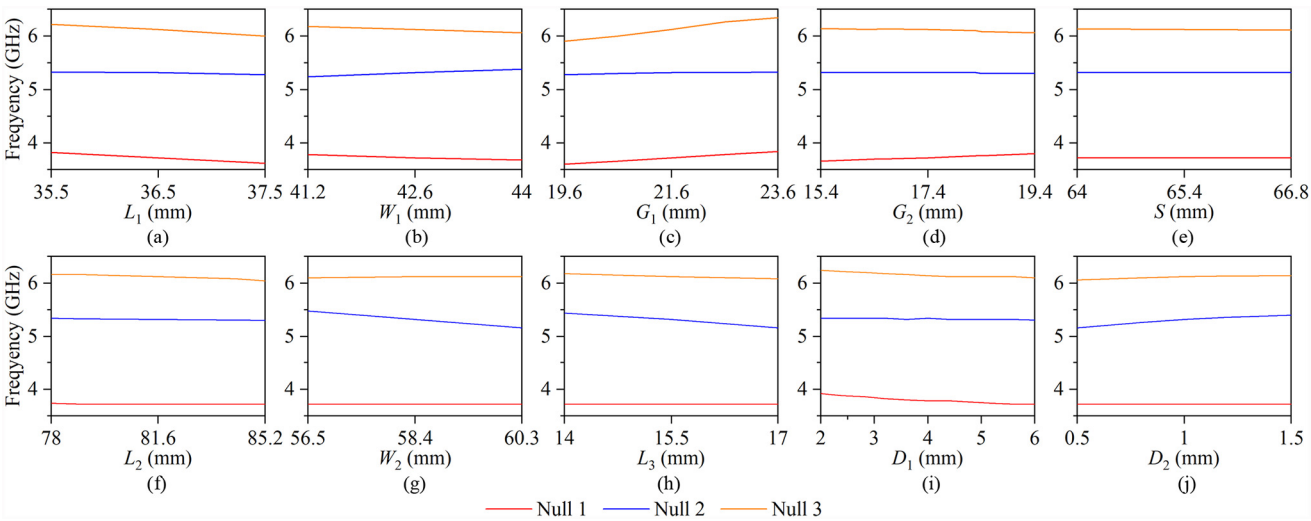

FIGURE 17. Variation of the null locations with respect to different dimensions of the antenna. (a) L_1. (b) W_1. (c) G_1. (d) G_2. (e) S. (f) L_2. (g) W_2. (h) L_3. (i) D_1. (j) D_2.

Different from the method for reshaping TM_{12} mode via adding shorting pins, the gain of TE_{23} mode is enhanced by removing a portion of pins surround the SIW cavity as shown in Fig. 3(d). Specifically, the removed shorting pins are located at both edges of the opposite outer sides of the SIW cavity and thus the original equivalent electric walls get truncated in their configuration. Herein, the same analytical method of the patch resonator is applied for the SIW cavity. Fig. 15 depicts the computed electric field of the modified SIW cavity. It is found that the positions with zero electric field along the radiation edges are shifted outward. Besides, the computed radiate and resonant performances of the modified SIW cavity are shown in Fig. 16, demonstrating the radiation of modified TE_{21} is well maintained while radiation of modified TE_{23} towards boresight direction is increased as L_3 is enlarged, i.e., more shorting pins removed. Besides, the resonant frequencies of modified TE_{21} and TE_{23} both decrease with the increase of L_3. The frequency responses of the finally designed antenna are given in Fig. 22 and it reveals that a stable realized gain above 8.2 dBi is indeed satisfactorily achieved in both passbands. Moreover, the influence of antenna parameters on three nulls is provided in Fig. 17, indicating the dimensions except the feeding location (S) all influence frequencies of radiation nulls. Such result is coincident with the producing

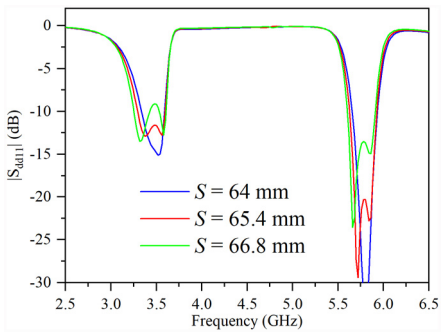

FIGURE 18. Simulated reflection coefficient of the antenna under different feeding locations (S).

principle of radiation nulls discussed above. Besides, from Fig. 18, it is known the locations of feeding probes mainly affect the impedance matching and a balance between the dual passbands is achieved when $S = 65.4$ mm.

C. EXTRACTION OF COUPLING MATRIX

Till now, the working mechanism of the proposed antenna has been intensively clarified and relevant dimensions have been studied. For further evident demonstration of the nulls, the coupling matrix of the proposed antenna is extracted herein.

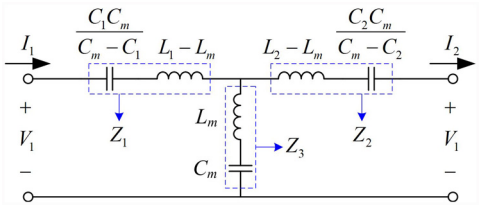

FIGURE 19. Transformed equivalent circuit of asynchronously tuned coupled resonators with the mixed electric coupling and magnetic coupling.

1) COUPLING EFFICIENT

For the upper band, both electric and magnetic couplings exist between the patch resonator and SIW cavity. In this case, the equivalent circuit model is depicted in Fig. 19. The two resonant frequencies of uncoupled resonators are deduced as $\omega_{01} = (L_1C_1)^{-1/2}$ and $\omega_{01} = (L_2C_2)^{-1/2}$ respectively. The electric and magnetic couplings are denoted as mutual capacitance C_m and inductance L_m.

For the equivalent T-type two-port network, the *ABCD* parameters of the transfer matrix is derived as

$$A = 1 + \frac{Z_1}{Z_3}, B = Z_1 + Z_2 + \frac{Z_1Z_2}{Z_3}, C = \frac{1}{Z_3}, D = 1 + \frac{Z_2}{Z_3} \tag{6}$$

where

$$\begin{aligned} Z_1 &= j\omega(L_1 - L_m) + 1/\left(j\omega\frac{C_1C_m}{C_m - C_1}\right) \\ Z_2 &= j\omega(L_2 - L_m) + 1/\left(j\omega\frac{C_2C_m}{C_m - C_2}\right) \\ Z_3 &= j\omega L_m + 1/(j\omega C_m) \end{aligned} \tag{7}$$

Then, the *S* parameters can be expressed in terms of *ABCD* parameters as

$$\begin{aligned} S_{11} &= \frac{A + B/Z_0 - CZ_0 - D}{A + B/Z_0 + CZ_0 + D} \\ S_{12} &= \frac{2(AD - BC)}{A + B/Z_0 + CZ_0 + D} \end{aligned} \tag{8}$$

At natural resonance, the reflection coefficient S_{11} is zero. After some manipulations, we can get

$$\omega_1 = \sqrt{\frac{\Re_B - \Re_C}{\Re_A}}, \omega_2 = \sqrt{\frac{\Re_B + \Re_C}{\Re_A}} \tag{9}$$

with

$$\begin{aligned} \Re_A &= 2\left(C_1C_2C_m^2L_1L_2 - C_1C_2C_m^2L_m^2\right)/\left(C_m^2 - C_1C_2\right) \\ \Re_B &= \left(C_1C_m^2L_1 + C_2C_m^2L_2 - 2C_1C_2C_mL_m\right)/\left(C_m^2 - C_1C_2\right) \\ \Re_C &= \sqrt{\Re_B^2 - 2\Re_A} \end{aligned} \tag{10}$$

Since $k_e = \sqrt{C_1C_2}/C_m$ and $k_m = L_m/\sqrt{L_1L_2}$, by substitution, the k_e and k_m can be derived from (9)-(10) as

$$k_m = \sqrt{\frac{b \pm c}{a}}, k_e = \frac{\omega_{02}^2 + \omega_{01}^2 - \left(\omega_2^2 + \omega_1^2\right)\left(1 - k_m^2\right)}{2\omega_{01}\omega_{02}k_m} \tag{11}$$

With

$$\begin{aligned} a &= 2\frac{\left(\omega_2^2 - \omega_1^2\right)^2}{\left[\left(\omega_{02}^2 + \omega_{01}^2\right) - \left(\omega_2^2 + \omega_1^2\right)\right]^2} \\ b &= 2\frac{2\omega_{01}^2\omega_{02}^2 - \left(\omega_{02}^2 + \omega_{01}^2\right)\left(\omega_2^2 + \omega_1^2\right) + \left(\omega_2^4 + \omega_1^4\right)}{\left[\left(\omega_{02}^2 + \omega_{01}^2\right) - \left(\omega_2^2 + \omega_1^2\right)\right]^2} \\ c &= \sqrt{b^2 - 2a} \end{aligned} \tag{12}$$

Then, the coupling efficient k can be obtained by [31]

$$k = (k_m - k_e)/(1 - k_mk_e) \tag{13}$$

Besides, for realization of transmission zero, it requires the transmission coefficient S_{12} to be zero and thus we obtain

$$\omega_m = \sqrt{\frac{k_e}{k_m}\omega_{01}\omega_{02}}. \tag{14}$$

2) EXTERNAL QUALITY FACTOR

The external quality factor Q_e can be obtained from the phase response of S_{11} and calculated by [37]

$$Q_e = \omega_0/\Delta\omega_{\pm 90^\circ} \tag{15}$$

where ω_0 is the resonant frequency and $\Delta\omega_{\pm 90^\circ}$ is the absolute bandwidth between the phase shift $\pm 90^\circ$ with respect to the absolute phase at ω_0.

3) UNLOADED QUALITY FACTOR

The unloaded quality factor can be calculated from the reflection coefficient [38]. Firstly, from the dip of the reflection coefficient, resonant frequency f_L and its magnitude $S_{11}^{\min}$ can be achieved. Accordingly, the coupling coefficient k can be calculated in terms of $S_{11}^{\min}$ as

$$k = \frac{1 - 10^{S_{11}^{\min}/20}}{1 + 10^{S_{11}^{\min}/20}} \quad \text{if the resonator is under coupled} \tag{16}$$

$$k = \frac{1 + 10^{S_{11}^{\min}/20}}{1 - 10^{S_{11}^{\min}/20}} \quad \text{if the resonator is over coupled} \tag{17}$$

Then, to determine the frequencies f_1 and f_2 which correspond to $S_{11} = S_{11}^{\phi}$, S_{11}^{ϕ} is found using

$$S_{11}^{\phi} = 10\log\frac{1 + 10^{S_{11}^{\min}/10}}{2} \tag{18}$$

Finally, the unloaded quality factor Q_u is calculated as

$$Q_u = (1 + k)f_L/(f_2 - f_1) \tag{19}$$

According to (6)-(19), the coupling matrix of the proposed antenna can be obtained. The extracted coupling matrices together with their corresponding frequency responses of both passbands are given in Fig. 20. As shown, for the lower passband, a transmission zero exists in the upper stopband. Similarly, there also has a transmission zero in the upper stopband of the upper passband. Moreover, the mixed coupling of the upper passband produces another transmission zero at the lower stopband edge of 5.20 GHz despite it cannot

TABLE 2. Comparison in various performances with other reported dual-band antennas.

	Dimensions	Profile	Layer	Operating Frequencies (GHz)	Bandwidth S_{11} < -10 dB (%)	Peak Gain (dBi)	Polarization	Filtering response	Radiation nulls
[22]	$0.72\lambda_0\times0.72\lambda_0$	$0.032\lambda_0$	3	3.6/5.2	4.2/3.8	7.5/8	LP/LP	Y	0
[24]	$0.63\lambda_0\times0.51\lambda_0$	$0.010\lambda_0$	1	1.9/2.6	2.1/1.9	6.7/7.3	LP/LP	Y	4
[25]	$\pi\times0.68\lambda_0\times0.68\lambda_0$	$0.072\lambda_0$	3	2.4/5.25	9.2/4.7	4.3/6.5	RHCP/LP	Y	4
[26]	$0.85\lambda_0\times0.85\lambda_0$	$0.025\lambda_0$	2	3.2/3.67	2.6/1.52	5.83/4.44	LP/LP	Y	2
[32]	$\pi\times0.21\lambda_0\times0.21\lambda_0$	$0.181\lambda_0$	2	2.05/3.5	10.1/3.73	1.18/0	LP/LP	Y	4
[33]	$0.88\lambda_0\times0.76\lambda_0$	$0.039\lambda_0$	2	3.6/4.1	2.3/1.6	4.84/4.85	LP/LP	Y	3
[34]	$1.06\lambda_0\times1.04\lambda_0$	$0.025\lambda_0$	1	2.52/3.43	2.77/3.49	7.9/8.55	LP/LP	Y	3
This work	$0.97\lambda_0\times0.7\lambda_0$	$0.037\lambda_0$	1	3.5/5.8	9.4/5.2	8.7/9.2	LP/LP	Y	3

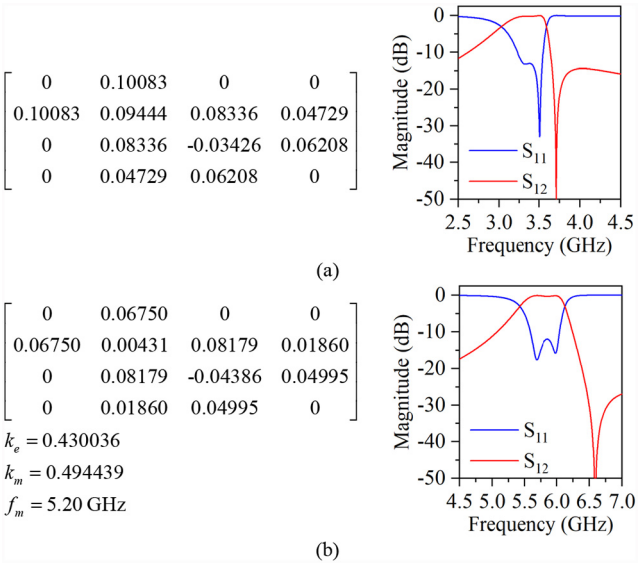

FIGURE 20. The extracted coupling matrices of the proposed antenna. (a) Lower passband. (b) Upper passband.

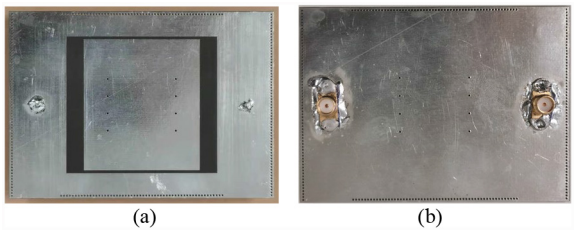

FIGURE 21. Photography of the fabricated dual-band filtering hybrid antenna. (a) Top view. (b) Side view.

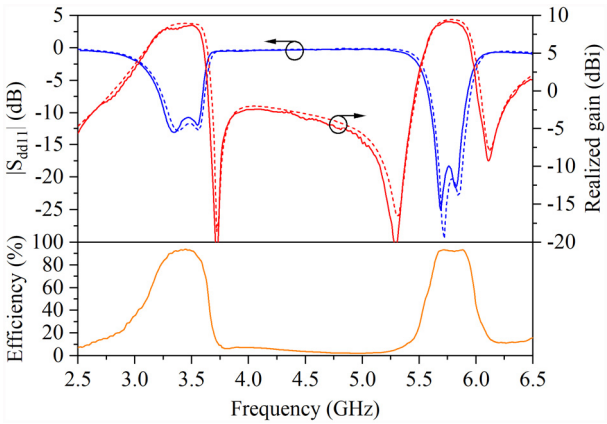

FIGURE 22. Simulated (dash line) and measured (solid line) results of the proposed dual-band hybrid filtering antenna.

be observed directly from frequency response curves. The obtained results are consistent with the frequency responses of the proposed antenna.

III. RESULTS AND EXPERIMENTAL VALIDATION

To confirm the above design method, the proposed dual-band filtering antenna is finally fabricated for experimental validation. The photograph of the fabricated antenna is given in Fig. 21. Its reflection coefficient is measured by using the Agilent N5230A vector network analyzer, while the radiation patterns and gains are obtained by using the near-field SATIMO antenna test system. The measured and simulated results are found in good accordance with each other as illustrated in Fig. 22 and Fig. 23.

Fig. 22 depicts the simulated and measured frequency responses of reflection coefficients, radiation gains, and efficiency. The measured results indicate that the antenna has satisfactorily gained an improved bandwidth ($|S_{dd11}| < -10$ dB) with two attenuation poles of about 9.4% (3.26-3.58 GHz) and 5.2% (5.60-5.90 GHz) in the lower and upper frequency bands, respectively. In this context, the overall thickness of this antenna is kept as small as around 0.037 λ_0 (λ_0 is the free space wavelength at 3.5 GHz which is the operation frequency of the lower passband), revealing its attractive low-profile property. Besides, the measured realized gains are slightly changed in the range of 8.1 to 8.7 dBi in the lower band and in the range of 7.9 to 9.2 dBi in the upper band, respectively, exhibiting relatively stable radiation gains in these dual passbands. Moreover, the radiation efficiency is higher than 90% over both passbands. Fig. 23 plots the simulated and measured radiation patterns of the designed dual-band filtering antenna. As can be seen herein, stable broadside radiation characteristics have been satisfactorily attained at all these four resonant frequencies.

In final, a comprehensive comparison has been conducted as tabulated and summarized in Table 2. It has been revealed herein that the proposed and designed dual-band filtering antenna indeed acquires the low profile, wide bandwidth, simple structure, and stable radiation compared with the reported works.

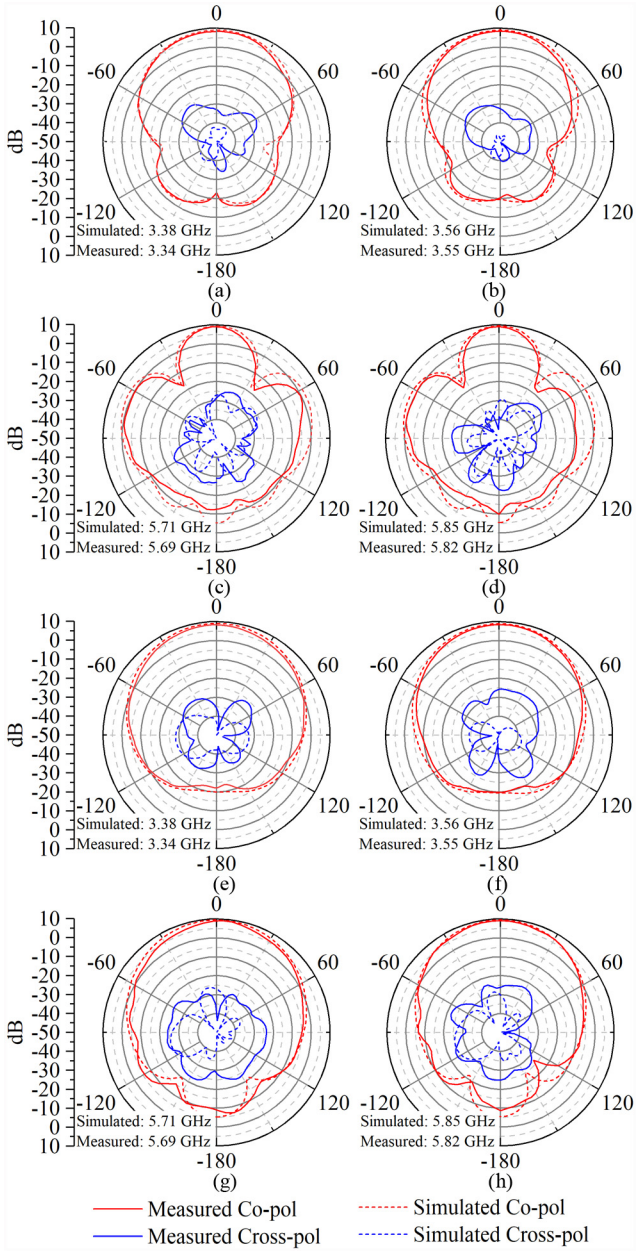

FIGURE 23. Simulated and measured radiation patterns of the proposed dual-band filtering hybrid antenna. (a)-(d) E-plane. (e)-(h) H-plane.

IV. CONCLUSION

In this paper, a dual-band filtering antenna is proposed based on the patch resonator and SIW cavity. By loading shorting pins in the rectangular patch resonator, the radiation performances of its first two odd modes are consistently maintained and a dual-band response for radiation is thus achieved. After that, the modified rectangular patch resonator is embedded within the rectangular SIW cavity for size compactness. With this arrangement, multiple resonant modes within these two resonators are properly generated and thus broaden the bandwidths of dual passbands. Meanwhile, since the cascaded trisection composed of the SIW cavity, the patch resonator, and the radiation impedance which represents the radiation of two resonators, together with the mixed coupling between the two resonators, three radiation nulls are produced, thus highly improving the frequency selectivity of both passbands. Then, to further obtain stable gain in the upper passband, a certain portion of the shorting pins surround the SIW cavity is appropriately removed. In final, an antenna prototype is fabricated and measured to validate the predicted results in a wide frequency range covering the dual passbands of our concern. Overall, the proposed antenna has been well exhibited to possess a few attractive performances, including dual-band radiation, stable gain, low profile, high selectivity, and compact configuration.

REFERENCES

[1] J. Tak, S. Woo, J. Kwon, and J. Choi, "Dual-band dual-mode patch antenna for on-/off-body WBAN communications," *IEEE Antennas Wireless Propag. Lett.*, vol. 15, pp. 348–351, 2015.

[2] T.-W. Chiou and K.-L. Wong, "A compact dual-band dual-polarized patch antenna for 900/1800-MHz cellular systems," *IEEE Trans. Antennas Propag.*, vol. 51, no. 8, pp. 1936–1940, Aug. 2003

[3] X. L. Bao and M. J. Ammann, "Dual-frequency circularly-polarized patch antenna with compact size and small frequency ratio," *IEEE Trans. Antennas Propag.*, vol. 55, no. 7, pp. 2104–2107, Jul. 2007.

[4] H. Yang, Y. Fan, and X. Liu, "A compact dual-band stacked patch antenna with dual circular polarizations for BeiDou navigation satellite systems," *IEEE Antennas Wireless Propag. Lett.*, vol. 18, pp. 1472–1476, 2019.

[5] M. Stanley *et al.*, "A dual-band dual-polarized stacked patch antenna for 28 GHz and 39 GHz 5G millimeter-wave communication," in *Proc. 13th Eur. Conf. Antennas Propag. (EuCAP)*, Krakow, Poland, 2019, pp. 1–4.

[6] X.-W. Dai, T. Zhou, and G.-F. Cui, "Dual-band microstrip circular patch antenna with monopolar radiation pattern," *IEEE Antennas Wireless Propag. Lett.*, vol. 15, pp. 1004–1007, 2016.

[7] A. A. Salih and M. S. Sharawi, "A dual-band highly miniaturized patch antenna," *IEEE Antennas Wireless Propag. Lett.*, vol. 15, pp. 1783–1786, 2016.

[8] H. Al-Saedi, J. A. Attari, W. M. A. Wahab, R. Mittra, and S. Safavi-Naeini, "Single-feed dual-band aperture-coupled antenna for 5G applications," in *Proc. 18th Int. Symp. Antenna Technol. Appl. Electromagn. (ANTEM)*, Waterloo, ON, Canada, 2018, pp. 1–2.

[9] M. Veysi, M. Kamyab, and A. Jafargholi, "Single-feed dual-band dual-linearly-polarized proximity-coupled patch antenna," *IEEE Antennas Propag. Mag.*, vol. 53, no. 1, pp. 90–96, Feb. 2011.

[10] C.-H. Chen and E. K. N. Yung, "A novel unidirectional dual-band circularly-polarized patch antenna," *IEEE Trans. Antennas Propag.*, vol. 59, no. 8, pp. 3052–3057, Aug. 2011.

[11] Nasimuddin, Z. N. Chen, and X. Qing, "Dual-band circularly polarized *S*-shaped slotted patch antenna with a small frequency-ratio," *IEEE Trans. Antennas Propag.*, vol. 58, no. 6, pp. 2112–2115, Jun. 2010

[12] W. C. Mok, S. H. Wong, K. M. Luk, and K. F. Lee, "Single-layer single-patch dual-band and triple-band patch antennas," *IEEE Trans. Antennas Propag.*, vol. 61, no. 8, pp. 4341–4344, Aug. 2013.

[13] Y. Li, Z. Zhao, Z. Tang, and Y. Yin, "Differentially fed, dual-band dual-polarized filtering antenna with high selectivity for 5G sub-6 GHz base station applications," *IEEE Trans. Antennas Propag.*, vol. 68, no. 4, pp. 3231–3236, Apr. 2020.

[14] D. E. Brocker, Z. H. Jiang, M. D. Gregory, and D. H. Werner, "Miniaturized dual-band folded patch antenna with independent band control utilizing an interdigitated slot loading," *IEEE Trans. Antennas Propag.*, vol. 65, no. 1, pp. 380–384, Jan. 2017.

[15] Q. Hou, H. Tang, Y. Liu, and X. Zhao, "Dual-frequency and broadband circular patch antennas with a monopole-type pattern based on epsilon-negative transmission line," *IEEE Antennas Wireless Propag. Lett.*, vol. 11, pp. 442–445, 2012.

[16] Y. Dong, H. Toyao, and T. Itoh, "Compact circularly-polarized patch antenna loaded with metamaterial structures," *IEEE Trans. Antennas Propag.*, vol. 59, no. 11, pp. 4329–4333, Nov. 2011.

[17] W. Cao, A. Liu, B. Zhang, T. Yu, and Z. Qian, "Dual-band spiral patch-slot antenna with omnidirectional CP and unidirectional CP properties," *IEEE Trans. Antennas Propag.*, vol. 61, no. 4, pp. 2286–2289, Apr. 2013.
[18] Z.-X. Liu, L. Zhu, and N.-W. Liu, "Design approach for compact dual-band dual-mode patch antenna with flexible frequency ratio," *IEEE Trans. Antennas Propag.*, vol. 68, no. 8, pp. 6401–6406, Aug. 2020.
[19] N.-W. Liu, L. Zhu, Z.-X. Liu, and Y. Liu, "Dual-band single-layer microstrip patch antenna with enhanced bandwidth and beamwidth based on reshaped multiresonant modes," *IEEE Trans. Antennas Propag.*, vol. 67, no. 11, pp. 7127–7132, Nov. 2019.
[20] P. Squadrito, S. Zhang, and G. F. Pedersen, "Wideband or dual-band low-profile circular patch antenna with high-gain and sidelobe suppression," *IEEE Trans. Antennas Propag.*, vol. 66, no. 6, pp. 3166–3171, Jun. 2018.
[21] C.-Y. Hsieh, C.-H. Wu, and T.-G. Ma, "A compact dual-band filtering patch antenna using step impedance resonators," *IEEE Antennas Wireless Propag. Lett.*, vol. 14, pp. 1056–1059, 2015.
[22] C. X. Mao *et al.*, "Dual-band patch antenna with filtering performance and harmonic suppression," *IEEE Trans. Antennas Propag.*, vol. 64, no. 9, pp. 4074–4077, Sep. 2016.
[23] Y. Yao, Z.-H. Tu, and Z. Gan, "An integration of dual-band filtering antenna for WLAN application," in *Proc. IEEE Int. Conf. Ubiquitous Wireless Broadband (ICUWB)*, Nanjing, China, 2016, pp. 1–3.
[24] X. Y. Zhang, Y. Zhang, Y.-M. Pan, and W. Duan, "Low-profile dual-band filtering patch antenna and its application to LTE MIMO system," *IEEE Trans. Antennas Propag.*, vol. 65, no. 1, pp. 103–113, Jan. 2017.
[25] B. Xiang, C. Wang, and S. Zheng, "A dual-band filtering antenna with different polarizations over two bands," in *Proc. Cross Strait Quad-Regional Radio Sci. Wireless Technol. Conf. (CSQRWC)*, Taiyuan, China, 2019, pp. 1–3.
[26] M.-Y. Xie and Z.-M. Xie, "A compact dual-band filtering antenna with high selectivity," in *Proc. Int. Conf. Microw. Millim. Wave Technol. (ICMMT)*, Guangzhou, China, 2019, pp. 1–3.
[27] W. Wang, C. Chen, and W. Wu, "Dual-band omnidirectional filtering antenna with high selectivity," in *Proc. IEEE MTT-S Int. Microw. Biomed. Conf. (IMBioC)*, Nanjing, China, 2019, pp. 1–3.
[28] H. Zhu, Y. Fan, X. Liu, and M. M. Tentzeris, "A compact, low-profile dual-band patch filtering antenna for off-body communications," in *Proc. Int. Appl. Comput. Electromagn. Soc. Symp. China (ACES)*, Beijing, China, 2018, pp. 1–2.
[29] C. Ma and S. Zheng, "A dual-band filtering antenna with a large frequency ratio," in *Proc. IEEE Int. Workshop Electromagn. (iWEM)*, Makung, Taiwan, 2020, pp. 1–2.
[30] A. Boualleg and N. Merabtine, "Analysis of radiation patterns of rectangular microstrip antennas with uniform substrate," *Semicond. Phys. Quantum Electron. Optoelectron.*, vol. 8, no. 3, pp. 88–91, 2005.
[31] Q.-X. Chu and H. Wang, "A compact open-loop filter with mixed electric and magnetic coupling," *IEEE Trans. Microw. Theory Techn.*, vol. 56, no. 2, pp. 431–439, Feb. 2008.
[32] P. F. Hu, Y. M. Pan, K. W. Leung, and X. Y. Zhang, "Wide-/dual-band omnidirectional filtering dielectric resonator antennas," *IEEE Trans. Antennas Propag.*, vol. 66, no. 5, pp. 2622–2627, May 2018.
[33] D. Zhao, F. Lin, H. Sun, and X. Y. Zhang, "A miniaturized dual-band SIW filtering antenna with improved out-of-band suppression," *IEEE Trans. Antennas Propag.*, early access, Jul. 2021, doi: 10.1109/TAP.2021.3098561.
[34] L. Li, S. Wu, D. Pang, X. Zhang, and Q. Wang, "A fifth-order single-layer dual-band half-mode SIW filtering antenna with a multi-functional single slot," *IEEE Antennas Wireless Propag. Lett.*, vol. 20, pp. 1676–1680, 2021.
[35] R. Garg, P. Bhartia, I. Bahl, and A. Ittipiboon, *Microstrip Antenna Design Handbook*. Boston, MA, USA: Artech House, 2001.
[36] D. M. Pozar, *Microwave Engineering*, 4th ed. New York, NY, USA: Wiley, 2011.
[37] J.-S. Hong, *Microstrip Filters for RF/Microwave Applications*. New York, NY, USA: Wiley, 2001.
[38] R. J. Cameron, C. M. Kudsia, and R. R. Mansour, *Microwave Filters for Communication Systems: Fundamentals, Design, and Applications*. New York, NY, USA: Wiley, 2007, ch. 11.

QIANWEN LIU received the B.Eng. and Ph.D. degrees from the Nanjing University of Science and Technology, Nanjing, China, in 2014 and 2020, respectively.

In 2017 and 2019, she was a Research Assistant with the Faculty of Science and Technology, University of Macau, Macau, SAR, China. She joined the College of Telecommunications and Information Engineering, Nanjing University of Posts and Telecommunications, Nanjing, China, as a Lecturer in December 2020. Her research interests include microwave circuits and antennas.

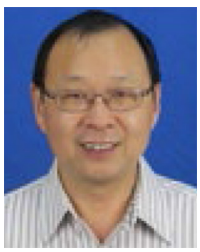

LEI ZHU (Fellow, IEEE) received the B.Eng. and M.Eng. degrees in radio engineering from the Nanjing Institute of Technology (currently, Southeast University), Nanjing, China, in 1985 and 1988, respectively, and the Ph.D. degree in electronic engineering from the University of Electro-Communications, Tokyo, Japan, in 1993.

From 1993 to 1996, he was a Research Engineer with Matsushita–Kotobuki Electronics Industries Ltd., Tokyo. From 1996 to 2000, he was a Research Fellow with the École Polytechnique de Montréal, Montréal, QC, Canada. From 2000 to 2013, he was an Associate Professor with the School of Electrical and Electronic Engineering, Nanyang Technological University, Singapore. He joined the Faculty of Science and Technology, University of Macau, Macau, China, as a Full Professor in August 2013, and has been a Distinguished Professor since December 2016. From August 2014 to August 2017, he served as the Head of Department of Electrical and Computer Engineering, University of Macau. He has authored or coauthored more than 600 papers in international journals and conference proceedings. His papers have been cited more than 10,720 times with the H-index of 53 (source: Scopus). His research interests include microwave circuits, antennas, periodic structures, and computational electromagnetics.

Prof. Zhu was the recipient of the 1997 Asia–Pacific Microwave Prize Award, the 1996 Silver Award of Excellent Invention from Matsushita–Kotobuki Electronics Industries Ltd., the 1993 Achievement Award in Science and Technology (First Prize) from the National Education Committee of China, the 2020 FST Research Excellence Award from the University of Macau, and the 2020 Macao Natural Science Award (Second Prize) from the Science and Technology Development Fund (FDCT), Macau. He served as the General Chair of the 2008 IEEE MTT-S International Microwave Workshop Series on the Art of Miniaturizing RF and Microwave Passive Components, Chengdu, China, and the Technical Program Committee Co-Chair of the 2009 Asia–Pacific Microwave Conference, Singapore. He was the Associate Editor for the IEEE TRANSACTIONS ON MICROWAVE THEORY AND TECHNIQUES from 2010 to 2013 and IEEE MICROWAVE AND WIRELESS COMPONENTS LETTERS from 2006 to 2012. He served as the member of IEEE MTT-S Fellow Evaluation Committee from 2013 to 2015, and the IEEE AP-S Fellows Committee from 2015 to 2017).